IOP Publishing Journal of Physics D: Applied Physics
J. Phys. D: Appl. Phys. **40** (2007) 4418–4424 doi:10.1088/0022-3727/40/15/005

Target-field method for MRI biplanar gradient coil design

Wentao Liu[1], Donglin Zu[1,3], Xin Tang[1] and Hua Guo[2]

[1] Institute of Heavy Ion Physics, Beijing Key Laboratory of Medical Physics and Engineering, Physics School, Peking University, Beijing 100871, People's Republic of China
[2] Siemens Mindit Magnetic Resonance Ltd, Shenzhen 518057, China

E-mail: dlzu@pku.edu.cn and dlzu@mpe.pku.edu.cn

Received 17 April 2007, in final form 4 June 2007
Published 13 July 2007
Online at stacks.iop.org/JPhysD/40/4418

Abstract
Based on the target-field method of solving Fredholm integral equations of the first kind, a new approach is presented in the paper for designing gradient coils that can be used in a permanent-magnet magnetic resonance imaging (MRI) system with biplanar poles. To restrict the current distribution on the coil plane within a finite radius, the current density is pre-expanded into Fourier series by orthogonal basis functions. By setting the target-field points and B_z values over the imaging region of interest, corresponding integral equations are derived from the Biot–Savart law to calculate the current densities. They form a matrix equation, in which the unknown elements of the column vector are the Fourier coefficients for the unknown current density. As long as these target-field points are well chosen, the Fourier coefficients can be solved by inverse matrix calculation instead of the regularization method for Fredholm integral equations of the first kind. Then the current density is discretized using the stream-function method to generate the winding patterns. To verify the feasibility of this approach, the gradient magnetic field generated by the current density is calculated via the Biot–Savart law. Optimized parameters are obtained through computer simulations for some shielded and unshielded transverse gradient coils. The performance of this approach has been demonstrated as well.

1. Introduction

It is a tremendous challenge for gradient coil design in magnetic resonance imaging (MRI) to generate a highly linear magnetic field gradient in a large space with a finite size coil while keeping small inductance and resistance, especially for an eddy current shielded gradient coil. The target-field method [1], proposed by Turner, has become the mainstream method not only for the cylinder-current-system gradient coil in superconducting MRI [2–5] but also for the biplanar gradient coil in permanent-magnet MRI [6]. However, the original Turner method [1] does not confine the current in a limited region since it employed Fourier transforms though his improved variant method [7] allows straightforward control of coil length in gradient coil designs. Extracting the current density distribution by solving the Fredholm integral equations of the first kind [8] is also a target-field method. Forbes and Crozier [9, 10] used this method to design finite-length shim coils for superconducting MRI, symmetric and asymmetric shimming and gradient coils for permanent-magnet MRI [11, 12]. Morrone's [13] method also belongs to this category.

To restrict the current distribution on the coil plane within a finite radius, the current density is pre-expanded into Fourier series via orthogonal basis functions. Then, with the target field set in the imaging region of interest, an integral equation is derived from the Biot–Savart law to calculate the current densities. Solving the integral equation is known as an inverse design problem. Since the integral equation is mathematically ill-conditioned, there is no unique solution generally. Forbes and Crozier [11, 12] used a regularization approach, similar to the Tikhonov method [8], to calculate the current density. Liu and Truwit [6] restricted the current in a square area by using Cartesian coordinates. Morrone [13] restricted the current in a circular area by using polar coordinates (the expression he

[3] Author to whom any correspondence should be addressed.

used for calculating the magnetic induction B_z is not correct). In this paper, we employ Morrone's trigonometric functions in the polar coordinate system as basis functions. Derived directly from the Biot–Savart law, the exact expression of B_z can be regarded as an integral equation for calculating the current densities when the magnetic induction field is specified in advance over some target regions. Mathematically, such an equation is known to be ill-conditioned, but we find that under certain physical and engineering conditions it is possible to get desired solutions by using a straightforward approach instead of using the Tikhonov regularization method [8].

2. Theory

In a permanent-magnet MRI system with biplanar poles, gradient and shim coils as well as RF transmitter coils are arranged on opposite planes. Among them the biplanar gradient coils are usually set in a finite region on planes at $z = \pm a$ and their radii ρ meets $\rho_0 < \rho < \rho_m$. Trigonometric functions in a circular polar coordinate system as basis functions are then used to express current density series [13]:

$$\begin{cases} J_\rho = \sum_{q=1}^{Q} U_q \frac{k}{\rho} \sin[qc(\rho - \rho_0)] \sin k\varphi, \\ J_\varphi = \sum_{q=1}^{Q} U_q qc \cos[qc(\rho - \rho_0)] \cos k\varphi, \end{cases} \quad (1)$$

where $c = \pi/(\rho_m - \rho_0)$, q and k are integers, ρ_0 is the minimum radius, ρ_m is the maximal radius, U_q is the current expansion coefficients, Q is the order of the expansion. We know from equation (1) that in the area of $\rho \leqslant \rho_0$ and $\rho \geqslant \rho_m$, $J_\rho = 0$, which ensures the current is confined within a finite area. The parameter k determines the order of the coils. It is only necessary to consider one k value at a time to design gradient coils and most shim coils. When $k = 0$, the current density can generate a longitudinal gradient field (z-gradient) or a constant magnetic field. When $k = 1$, the coils generate the transverse linear gradient field in either x or y direction. By rotating 90°, an x-gradient coil becomes a y-gradient coil. Shim coils can be obtained by setting $k \geqslant 2$. It must be emphasized that when $Q \to \infty$, equation (1) is determined by all levels of the current densities. When Q is a finite number, the finite order U_q can approximately determine the current density. The distribution of plane current density satisfies the two-dimensional equation of continuity

$$\nabla \cdot \vec{J} = \frac{1}{\rho}\left[\frac{\partial}{\partial\rho}(\rho J_\rho) + \frac{\partial J_\varphi}{\partial\varphi}\right] = 0. \quad (2)$$

2.1. Transverse gradient coils

The two plane coils, with current flowing within the circles, are at $z = \pm a$, respectively, as shown in figure 1. In polar coordinates, at the source point $P'(\rho, \varphi)$, the two components of the current density are J_ρ and J_φ, respectively. The two current planes generate a magnetic field, $\vec{B}$, at the field point $P(x, y, z)$ by the Biot–Savart law,

$$\vec{B}(x, y, z) = \frac{\mu_0}{4\pi}\int \frac{\vec{J} \times \vec{R}}{R^3} d\sigma', \quad (3)$$

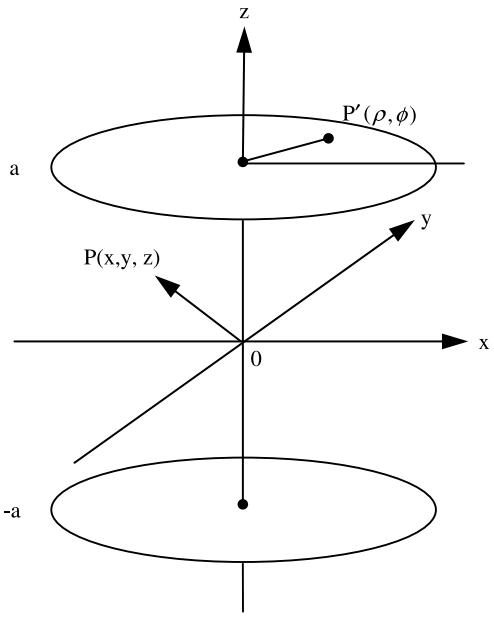

Figure 1. Biplanar gradient coils system.

where μ_0 is permeability of vacuum, $\vec{J}$ is the current density at the source point, $\vec{R}$ is the vector from the source point to the field point, $d\sigma'$ is the area element at the source point. Only the axial component of the magnetic field is interested here, which can be obtained from equation (3)

$$B_z(x, y, z) = \frac{\mu_0}{4\pi}\iint \frac{dx'\,dy'}{R^3}[J_x(y - y') - J_y(x - x')]. \quad (4)$$

In the polar coordinates system, it can be further expressed as

$$B_z = \frac{\mu_0}{4\pi}\int_{\rho_0}^{\rho_m}\int_0^{2\pi} \frac{\rho\, d\rho\, d\varphi}{R^3}[(J_\rho \cos\varphi - J_\varphi \sin\varphi)(y - \rho\sin\varphi) - (J_\rho \sin\varphi + J_\varphi \cos\varphi)(x - \rho\cos\varphi)]. \quad (5)$$

Setting the two planes $z = a$ and $z = -a$ as + and − planes, the sum magnetic field of two planes is

$$B_z = \frac{\mu_0}{4\pi}\int_{\rho_0}^{\rho_m}\int_0^{2\pi} \frac{\rho d\rho d\varphi}{R_+^3}[(J_\rho \cos\varphi - J_\varphi \sin\varphi)(y - \rho\sin\varphi) - (J_\rho \sin\varphi + J_\varphi \cos\varphi)(x - \rho\cos\varphi)] + \frac{\mu_0}{4\pi}\int_{\rho_0}^{\rho_m}\int_0^{2\pi} \frac{\rho d\rho d\varphi}{R_-^3}[(J_\rho \cos\varphi - J_\varphi \sin\varphi)(y - \rho\sin\varphi) - (J_\rho \sin\varphi + J_\varphi \cos\varphi)(x - \rho\cos\varphi)], \quad (6)$$

where $R_\pm = [(x - \rho\cos\varphi)^2 + (y - \rho\sin\varphi)^2 + (z \mp a)^2]^{1/2}$.

Equation (1) is series summation in terms of q. Substituting equation (1) with $k = 1$ in equation (6), B_z becomes

$$B_z = \sum_{q=1}^{Q} U_q \left\{\frac{\mu_0}{4\pi}\int_{\rho_0}^{\rho_m}\int_0^{2\pi} \frac{\rho\, d\rho d\varphi}{R_+^3}[(\sin\beta - qc\rho\cos\beta) \times (y - \rho\sin\varphi)\sin\varphi\cos\varphi\right.$$

$$
\begin{aligned}
&- (\sin\beta \sin^2\varphi + qc\rho \cos\beta \cos^2\varphi)(x - \rho\cos\varphi)] \\
&+ \frac{\mu_0}{4\pi} \int_{\rho_0}^{\rho_m} \int_0^{2\pi} \frac{\rho \mathrm{d}\rho \mathrm{d}\varphi}{R_-^3} [(\sin\beta - qc\rho\cos\beta) \\
&\times (y - \rho\sin\varphi)\sin\varphi\cos\varphi \\
&- (\sin\beta \sin^2\varphi + qc\rho \cos\beta \cos^2\varphi)(x - \rho\cos\varphi)]\Bigg\},
\end{aligned} \tag{7}
$$

where $\beta = qc(\rho - \rho_0)$.

The values of target-field points B_z can be predetermined, and the positions of these points are known. So according to equation (1), the current density can be determined by solving the coefficient U_q from equation (7). Herein we define an intermediate term

$$
\begin{aligned}
D_q = &\frac{\mu_0}{4\pi} \int_{\rho_0}^{\rho_m} \int_0^{2\pi} \frac{\rho \,\mathrm{d}\rho \,\mathrm{d}\varphi}{R_+^3} [(\sin\beta - qc\rho\cos\beta) \\
&\times (y - \rho\sin\varphi)\sin\varphi\cos\varphi \\
&- (\sin\beta \sin^2\varphi + qc\rho \cos\beta \cos^2\varphi)(x - \rho\cos\varphi)] \\
&+ \frac{\mu_0}{4\pi} \int_{\rho_0}^{\rho_m} \int_0^{2\pi} \frac{\rho \mathrm{d}\rho \mathrm{d}\varphi}{R_-^3} [(\sin\beta - qc\rho\ \cos\beta) \\
&\times (y - \rho\sin\varphi)\sin\varphi\cos\varphi \\
&- (\sin\beta \sin^2\varphi + qc\rho \cos\beta \cos^2\varphi)(x - \rho\cos\varphi)].
\end{aligned} \tag{8}
$$

Then equation (7) is written as

$$
B_z = \sum_{q=1}^{Q} U_q D_q, \tag{9}
$$

where the element D_q is just the function of the field point $P(x, y, z)$, B_z refers to the magnetic field at the point $P(x, y, z)$ and the element U_q is the coefficient of the current density series in equation (1). Writing a matrix form,

$$
\begin{bmatrix} B_1 \\ B_2 \\ B_3 \\ \vdots \\ B_Q \end{bmatrix} = \begin{bmatrix} D_{11} & D_{12} & D_{13} & \cdots & D_{1Q} \\ D_{21} & D_{22} & D_{23} & \cdots & D_{2Q} \\ D_{31} & D_{32} & D_{33} & \cdots & D_{3Q} \\ \vdots & \vdots & \vdots & \ddots & \vdots \\ D_{Q1} & D_{Q2} & D_{Q3} & \cdots & D_{QQ} \end{bmatrix} \begin{bmatrix} U_1 \\ U_2 \\ U_3 \\ \vdots \\ U_Q \end{bmatrix}. \tag{10}
$$

The linear algebra equations are equivalent to equation (7). By solving U_q in equation (10), the current density can be determined if at least Q target-field points are known.

2.2. Shielded transverse gradient coils

In a permanent-magnet MRI system, biplanar gradient coils are close to the iron-pole surface of the magnet. Consequently, the eddy currents become more serious than those in a superconducting MRI system. The most efficient way to deal with the eddy currents is to suppress the fields that cause them, which is the principle for designing shielded gradient coils. By using a couple of shield coils in the outer space of primary coils, the field generated counteracts the field from the primary coils to a minimum level. Assuming the shield coils are located at positions $z = \pm b$ $(b > a)$ as shown in figure 2, the expression of the current density on the shield coils is similar to that of the primary coils, and the coefficient of the series is supposed to be V_q. The B_z by the Biot–Savart law is written as

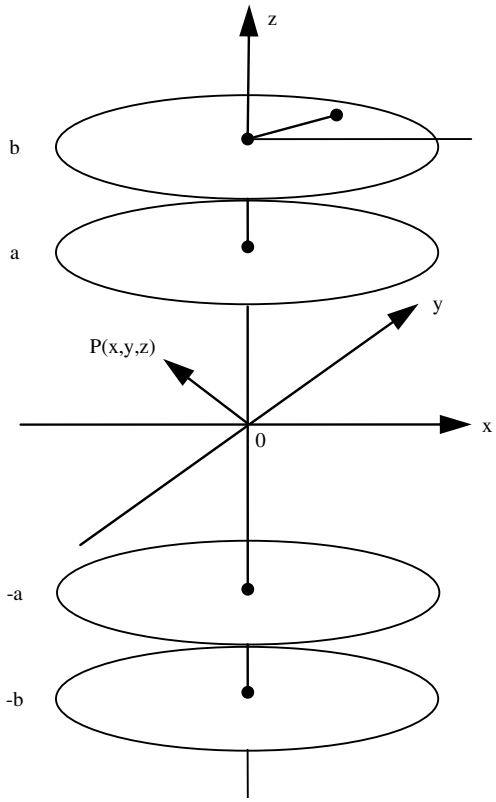

Figure 2. Shielded gradient coils system.

$$
B_z = \sum_{q=1}^{Q} U_q D_q + \sum_{q=1}^{P} V_q E_q. \tag{11}
$$

Similar to equation (9), the elements D_q and E_q are just the functions of the field point $P(x, y, z)$. With target-field points B_z defined first, there are $Q + P$ unknown variables in equation (11). Therefore $Q + P$ target points in the space of imaging region and shielding region are needed for solving the equation. Given the target points and the corresponding target values, B_i $(i = 1, 2, \ldots, Q + P)$, equation (11) is written as a matrix equation after calculating D_{iq} and E_{iq} from equation (8)

$$
\begin{bmatrix} B_1 \\ B_2 \\ \vdots \\ B_i \\ \vdots \\ B_{Q+p} \end{bmatrix} = \begin{bmatrix} D_{11} & \cdots & D_{1Q} & E_{11} & \cdots & E_{1P} \\ D_{21} & \cdots & D_{2Q} & E_{21} & \cdots & E_{2P} \\ \vdots & \ddots & \vdots & \vdots & \ddots & \vdots \\ D_{i1} & \cdots & D_{iQ} & E_{i1} & \cdots & E_{iP} \\ \vdots & \ddots & \vdots & \vdots & \ddots & \vdots \\ D_{Q+P1} & \cdots & D_{Q+PQ} & E_{Q+P1} & \cdots & E_{Q+PP} \end{bmatrix} \begin{bmatrix} U_1 \\ \vdots \\ U_Q \\ V_1 \\ \vdots \\ V_P \end{bmatrix}. \tag{12}
$$

Solving U_q and V_q from equation (12) by the same method as above, the current density in the primary and the shield coils can be determined at the same time.

Table 1. Parameters of transverse gradient coil with different Q indices.

Q	Max. departure from linearity (%)	Efficiency (mT m^{-1} A^{-1})	Number of turn	Number of small loops	Number of current oscillation	Inductance (mH)	Resistance (mΩ) (10 mm^2)
1	66.75	0.121	11	0	0	0.101	44.12
2	48.81	0.087	11	0	0	0.121	51.65
3	22.41	0.069	13	0	0	0.174	58.96
4	8.46	0.061	12	1	0	0.209	65.67
5	3.86	0.05	16	1	0	0.171	75.46
6	3.62	0.042	21	1	1	0.281	86.5
7	0.41	0.036	21	0	1	0.227	101.01
8	0.81	0.033	23	0	1	0.195	110.48
9	0.07	0.025	28	0	1	0.38	137.05
10	0.06	0.022	33	1	1	0.35	156.35
11	0.02	0.018	37	1	1	0.575	182.68
12	0.14	0.021	42	0	3	0.524	199.22

2.3. Generating winding patterns

From the distribution of current densities calculated above, the winding patterns can next be calculated by the stream-function method [14]. Since the current density satisfies the steady flow condition

$$\nabla \cdot \vec{J} = \frac{1}{\rho}\left[\frac{\partial}{\partial \rho}(\rho J_\rho) + \frac{\partial J_\varphi}{\partial \varphi}\right] = 0,$$

we can introduce the function $I(\rho, \varphi)$ on the coil planes

$$\begin{cases} \dfrac{\partial I(\rho,\varphi)}{\partial \rho} = -J_\varphi(\rho,\varphi) \\ \dfrac{\partial I(\rho,\varphi)}{\partial \varphi} = \rho J_\rho(\rho,\varphi). \end{cases} \tag{13}$$

According to equations (1) and (13), the stream function is found as follows:

$$I(\rho,\varphi) = -\sum_{q=1}^{Q} U_q \sin[qc(\rho-\rho_0)]\cos\varphi. \tag{14}$$

Assuming the coil on a half-circular plane consisting of N turns of wire, we choose a set of contours, $\{I(\rho,\varphi) = (i+1/2)I_0, i = 0, 1, 2, \ldots, N-1\}$, where $I_0 = I_{\max}/N$, and $I_{\max}$ refers to the maximal value of the stream function on the half-circular plane. The contours represent the winding patterns. Using the stream-function method, the current in every turn can be ensured equal to I_0. Additionally, the turn number N and the current I_0 can be controlled.

3. Results

In numerical simulation studies, parameters are chosen according to the practical design. The maximal radius of the gradient coils $\rho_m = 42$ cm, the maximal radius of the shield coils $\rho_{sm} = 50$ cm, the minimal radius $\rho_0 = 1$ cm, the distance between the gradient coil plane and the centre plane $a = 23$ cm, the distance between the shield-coil plane and the centre plane $b = 29$ cm (the distance between the gradient coil plane and the shield-coil plane is 6 cm). The imaging region of interest is a $40 \times 40 \times 30$ cm^3 spheroid, i.e. the coordinates x: −20 cm–20 cm, y: −20 cm–20 cm, z: −15 cm–15 cm. In the imaging region the goal gradient field G_i=25 mT m^{-1}, with $i = x, y, z$, respectively. The shielded region is the outboard space of the shield coils, set as $|z| \geqslant 29.5$ cm.

3.1. Transverse gradient coil

Due to the spatial symmetry of the biplanar transverse gradient coil system, magnetic field at each space point can be calculated by the space symmetry transform of the first octant ($x > 0$, $y > 0$, $z > 0$). Therefore, the target-field points need to be set only in the first octant. As a matter of fact, during simulation we find that if the target-field points are set at symmetric positions in other octants, the matrix equation appears seriously ill-conditioned, thereby lacking a solution. According to the design requirement, on grids of a 5 cm long cube, we choose 29 target points in the first octant with each target value set as $B_{zi} = G_x x_i$. Using the above target-field method, these U_q ($q = 1, 2, \ldots, N$; $N < 29$) values are found; then distributions of the current density are obtained, and the winding patterns are determined through the stream-function method. Theoretically, it seems necessary to set Q bigger than or equal to 29 to make the matrix equation solvable. However, in practice, for the gradient in the imaging volume, a certain tolerance (<5%) can be accepted and a reasonable Q to provide accurate solutions is enough.

A key concern is to determine appropriate numbers for the index Q in equation (1). Different Q determines different winding patterns, since there is no unique solution to this problem. We implement a series of simulations for Q from 1 to 12. The effectiveness of the coil design has been evaluated by calculating the magnetic fields. This is accomplished using the Biot–Savart law (8), given the computed current density components and stream functions. To compare the coils with almost the same gradient field in the imaging region, the simulation results are listed in table 1.

The table shows a trend that the linearity in the imaging region is getting better when Q increases. For a larger Q the coil can produce a gradient field exactly equal to the target field. At the same time, other parameters of the coils become worse as Q grows. These include the appearance of 'small loop' and current oscillation in the coil planes which leads to poorer efficiency, larger inductance and higher resistance. A larger inductance means the coil has a slower slew rate; and a higher resistance means the coil dissipates more power. Therefore, a compromise has to be made among these parameters. Here, as the requirement of maximum offset from linearity <5%, a coil with $Q = 5$ is the most optimal. For the typical case with $Q = 5$, figure 3(*c*) shows the winding pattern,

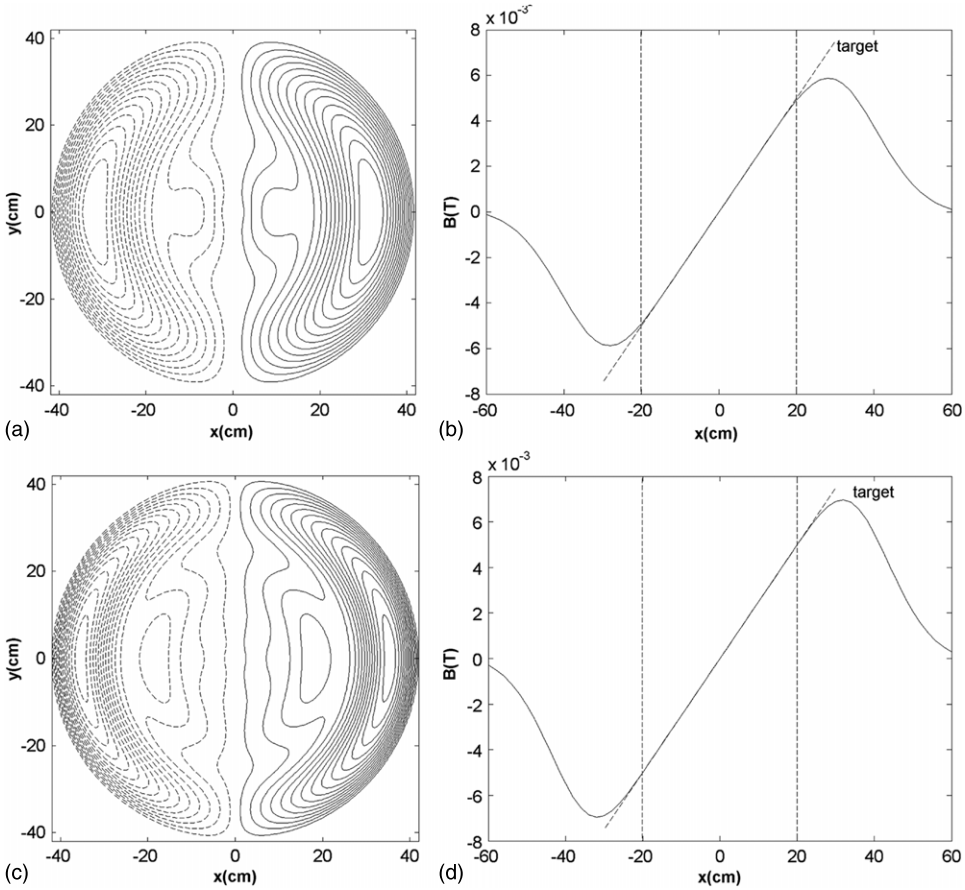

Figure 3. The winding pattern of the gradient coil with (*a*) $Q = 3$, (*c*) $Q = 5$, (*b*) the field (solid) along x-axis produced by the coil shown in (*a*) and (*d*) the field (solid) along x-axis produced by the coil shown in (*c*). The target field is shown as a skew dashed line, and the pair of vertical dashed lines indicate the positions that define the imaging region.

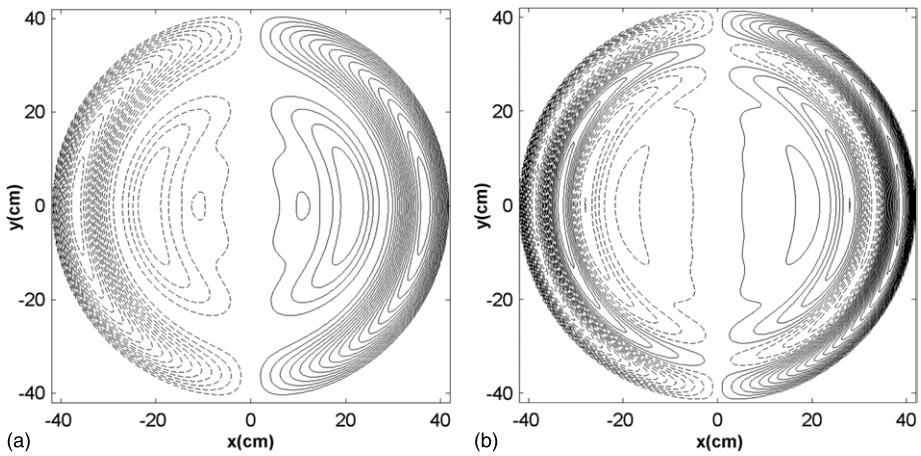

Figure 4. The winding pattern of unshielded gradient coil when $Q = 6$ (*a*) and $Q = 10$ (*b*).

and (*d*) shows the magnetic field component along the x-axis. Figure 3(*a*) and (*b*) show the case when $Q = 3$ for comparison. Higher degree of accuracy implies a bigger region with linear gradient. As Q increases, although the coil designed has a high degree of accuracy, the current on a half-circular plane oscillates as shown in figure 4. As a solution they are more accurate mathematically. However, such coils are not useful due to their low efficiency, large induction and resistance as well as manufacturing issues.

3.2. Shielded transverse gradient coil

According to the design requirement (imaging region is a $40 \times 40 \times 30\,\mathrm{cm}^3$ spheroid), 29 target points in the region of interest uniformly located on the grids of a 5 cm long cube are set in the first octant, and their target values are set as $B_i = G_x x_i$. The 40 restricting target field points in shielding space are set equidistantly at the plane $z = 29.5\,\mathrm{cm}$ ($x > 0$, $y > 0$), and the corresponding target values are set to zero.

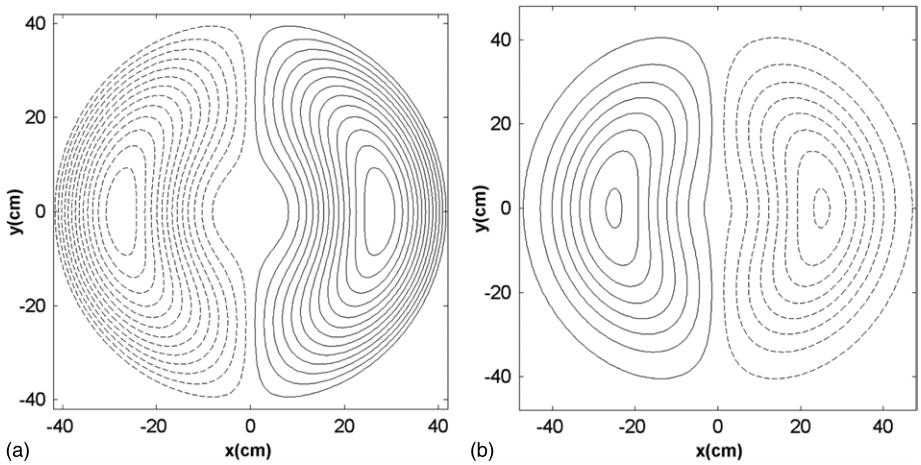

Figure 5. The winding patterns of shielded gradient coils with $Q = P = 3$: (a) the primary coil; (b) the shield coil. The distance between the primary coil and the shield coil is 6 cm.

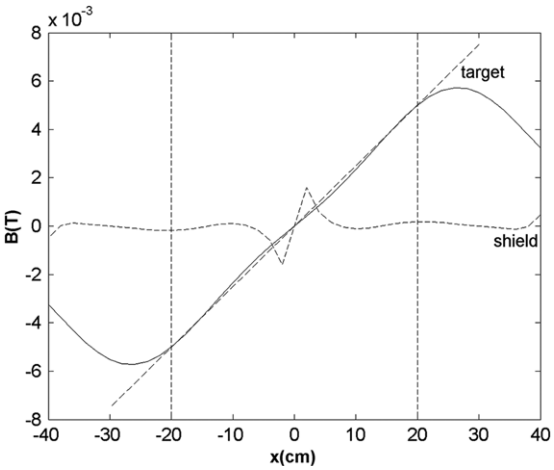

Figure 6. The field generated by shielded gradient coils when $Q = P = 3$.

When we come to solve the problem, indices Q and P are also the key concerns. Besides the linearity of the gradient field and the efficiency of the coils, the shielding efficiency in the outer space needs to be considered in the design. The general rule is that the bigger Q is, the better the linearity of the gradient field; the bigger P is, the higher the shielding efficiency in the outer space. In addition, P should not be smaller than Q for better shielding. However, the larger P and Q are the lower the coil efficiency is. It is important to note that in practice, the currents in the gradient and shield coil should be the same, since different currents need different sources, which are hard to be synchronized.

In the calculation, Q and P are set to 3; and the currents in all the coils are the same. The winding patterns of the primary and shield coils are illustrated in the figures 5(a) and (b), respectively. Dashed lines indicate reverse windings. The magnetic field generated by this coil is shown in figure 6. In the imaging region, the gradient field of $G_x = 25\,\mathrm{mT\,m^{-1}}$ requires the input current to be 500 A. The oblique dashed line stands for ideal gradient. The vertical dashed lines mark the boundary of the imaging region. The horizontal dashed line shows the magnetic field, which is close to zero, outside the shield coil ($z \geqslant 29.5$ cm). The gradient field has a good linearity (at $x = \pm 7$ cm, non-linearity $= 7.4\%$) in the imaging region while the field in the shielding region is well controlled. The efficiency of the coil system is $0.05\,\mathrm{mT\,m^{-1}\,A^{-1}}$ and there is no current oscillation.

4. Discussion

Generally, the forward problem of electromagnetic field has unique solutions. Inverse design problems using a Fourier-transform technique avoids the ill-posed nature since Fourier-transform has unique inverses. However, for finite size plates the integral equation technique has to face the ill-posed nature of the problem. The governing equations (6) and (7) are all integral equations derived from the Biot–Savart law. Given B_z-field values at discrete target points over the imaging volume the current densities on the opposite biplanar are the unknown variables to be found. The components J_ρ and J_φ are not independent and satisfy equation (2). Therefore, equations (6) and (7) belong to the typical Fredholm integral equations of the first kind. Their ill-posed nature may appear either without unique solutions, or unstable solutions, or even non-existent solutions. In other words, the ill-posed degree of these equations varies depending on the choice of the target-field points. For the equivalent matrix equations (10) and (12), the mathematical nature of the connectivity matrix is intimately connected with the choice of the target-field points. Our numerical simulations show that if the target-field points are set in the first octant, the problem is not ill-posed. Therefore it is possible to get desired solutions easily using matrix software instead of the standard Tikhonov regularization method [8]. Though there is no unique current density which satisfies each equation, the approximate current density can be obtained. When the index numbers Q in equations (1), (7), (9) and (10) are properly chosen (not very large), the approximate current density found through inverse matrix calculation meets the target field with reasonable accuracy. Nevertheless, outlined by equation (1), the increase in Q also leads to more frequent oscillation of the current density. The counteraction of the field caused by the frequently reversed current reduces the efficiency of the gradient coils and increases the difficulty in

manufacturing. Thereby, a compromise must be made between accuracy and efficiency. From this point of view, an absolutely accurate solution to the integral equation is not worth pursuing. The effectiveness of the coil design is assessed by calculating the magnetic field with the Biot–Savart law, which is used as a gold standard. According to the simulation results the region of linearity increases as Q increases. Consequently, to use the Tikhonov regularization [8–12] the Fredholm integral equations of the first kind is unnecessary. Moreover, the aim to use the Tikhonov regularization is to find a unique solution. Although the solution may be mathematically accurate, it is not likely to be the best one in terms of engineering. In addition, the regularizing parameters and the penalty functions can be freely chosen by designers according to their experience. As an alternative to the regularization approach, the method reported in this paper is efficient and convenient.

5. Conclusion

In summary, this paper provides a suite of simple approaches to design gradient coils, which can meet the requirement of linearity, for permanent-magnet MRI systems, while the geometry shape and size of the coil can be realized according to the design requirement. Moreover, eddy currents can be avoided by designing shielded coil systems. The method should also work for designing longitudinal gradient and shim coils.

Acknowledgments

The authors thank the two anonymous reviewers for their guidance in the development and presentation of this work.

References

[1] Turner R 1986 *J. Phys. D: Appl. Phys.* **19** 147–51
[2] Turner R 1988 *J. Phys. E: Sci. Instrum.* **21** 948–52
[3] Turner R 1993 *Magn. Reson. Imag.* **11** 903–20
[4] Chronik B A and Rutt B K 1998 *Magn. Reson. Med.* **39** 270
[5] Tang X, Zu D and Bao S 2004 *Prog. Nat. Sci.* **14** 753–7
[6] Liu H and Truwit C L 1998 *IEEE Trans. Med. Imag.* **17** 826–30
[7] Turner R 1992 *US Patent* **5** 289 151
[8] Groetsch C W 1984 *The Theory of Tikhonov Regularization for Fredholm Equations of the First Kind* (Boston, MA: Pitman)
[9] Forbes L K and Crozier S 2001 *J. Phys. D: Appl. Phys.* **34** 3447–55
[10] Forbes L K and Crozier S 2002 *J. Phys. D: Appl. Phys.* **35** 839–49
[11] Forbes L K and Crozier S 2004 *IEEE Trans. Magn.* **40** 1929–38
[12] Forbes L K, Brideson M and Crozier S 2005 *IEEE Trans. Magn.* **41** 2134–44
[13] Morrone T 1992 *US Patent* 5760582
[14] Tomasi D 2001 *Magn. Reson. Med.* **45** 505